RESEARCH ON THE STRUCTURAL DESIGN AND PATH TRACKING CONTROL ALGORITHM OF AN INTELLIGENT ROAD TRAFFIC MARKING ROBOT

Yanlin WANG[1,3], Yaozhou WANG[1,3], Junjie XIE[2], Hui DOU[2], Shenghao WU[1,3], Yuan HE[1,3], Wei LI[4,*] , Chunjie ZHANG[5]

In order to achieve fully automatic operation of various road marking tasks and improve the accuracy of the operation, an intelligent road traffic marking robot (IRTMR) is designed in this study, and its path tracking control algorithm is studied. Firstly, the structure of an IRTMR with two-component spraying was designed. Secondly, the kinematic and dynamic models of the IRTMR were established. The principle of the path tracking control algorithm for the IRTMR was analyzed based on the kinematic and dynamic models, and a path tracking controller was constructed. Finally, the control accuracy of the model predictive control (MPC) algorithm was studied through simulation experiments. The results show that the accuracy of the MPC algorithm is very good. The root mean square error of the MPC and the peak lateral error are 0.001319m *and* 0.006589m*, separately. The MPC algorithm can meet the accuracy requirements of the IRTMR for road traffic marking operation, which lays the foundation for the subsequent research on path tracking control testing of the prototype.*

Keywords: Intelligent road traffic marking robot, Two-component spraying, Path tracking algorithm, MPC algorithm

1. Introduction

The national standard GB 5768.3-2009 Road Traffic Signs and Markings has promoted the standardization and modernization of road traffic signs and markings in China [1]. With the continuous progress of science and technology, robots are gradually integrated into road traffic construction sector [2-8].

* Corresponding author

[1] Associate Professor, School of Mechanical and Electrical Engineering, Lanzhou University of Technology, Gansu, China, Email: wangyanlin@lut.edu.cn

[2] Gansu Road and Bridge Construction Group Co., Ltd., Lanzhou 730030, Gansu;

[3] Mechanical Industry Heavy-load Flexible Robot Key Laboratory, Lanzhou 730050, Gansu;

[4] Wuhan Railway Vocational College Of Technology，Wuhan，430205，Hubei;

[5] Lanzhou High-Speed Railway Infrastructure Section, China Railway Lanzhou Group Co., Ltd, Lanzhou 730050, Gansu

Compared with manual operation, the IRTMRs can significantly shorten the construction time and effectively improve the construction quality. Where, the trajectory tracking control technology is the key to ensure the operation accuracy of the IRTMR [9-11].

The fully autonomous operation study has attracted the research interest of scholars around the world. A mobile waterline robot named Tiny Surveyor developed by Denmark's Tiny Mobile Robots Company has an autonomous navigation function. It can accurately navigate along a predetermined path for waterline application tasks. RP company of South Korea developed a road marking robot called R-BOT [12] which utilizes natural language processing for automatic coordinate conversion, along with tilt coordinate conversion algorithms. It also features automatic uniform spraying technology according to designated spraying path. However, the above robots adopt cold spray scribing technology and hot melt scribing technology, respectively. There are somewhat lacking above robots in environmental protection. The American Graco [13] possesses this environmentally friendly technology, but they implement technological blockade against other countries mainly through patent protection, export restriction, market strategy, reduction of cooperation and strict technology transfer restriction, aiming to maintain its competitive advantage in the market. Therefore, it becomes very important to develop a new IRTMR. In this study, two-component waterborne markings constructed by ambient- friendly spraying are characterized by low volatile and organic compound emissions, energy saving, environmental protection, and superior performance [14-18], and the carbon emissions are reduced by 80% compared with traditional hot-melt markings.

The path tracking control is an important part of the IRTMR to achieve road marking application [19]. Wang et al. [20] proposed a pre-acquisition tracking fuzzy control algorithm, which takes lateral deviation and heading deviation as input parameters of a multi-input-output fuzzy controller to achieve parallel control of steering and straight line travelling of a vehicle in the same control cycle. Fu et al. [21] proposed an unmanned vehicle path tracking algorithm based on an improved Pure Pursuit model to solve the problem of large errors in tracking the ideal path with the predicted forward-looking distance set by the traditional Pure Pursuit algorithm. Zhou et al. [22] proposed an improved linear quadratic regulator (LQR) path-tracking lateral control strategy in order to solve the problem that it is difficult for intelligent vehicles to simultaneously ensure control accuracy and safety margin when passing through curves or narrow regions. Cui et al. [23] determined the gain coefficients of the control model in

real-time by constructing the affiliation function with lateral deviation and heading deviation as input variables and designing a fuzzy inference and defuzzification process to enhance the adaptive capability of Stanley's model on different curvature paths. The lateral errors of the path-tracking control algorithms studied above have large control errors greater than 1cm.

In order to address the above problems, the Pure Pursuit Algorithm, Stanley algorithm, Linear Quadratic Regulator algorithm, and MPC algorithm are investigated this study, respectively. Path tracking control algorithms are investigated, and simulation experiments are carried out by setting up more complex paths with the same parameters. As the IRTMR is mainly used in highway construction sites, the IRTMR adopts low-speed driving to ensure that the speed is controlled within 5 km/h, and the lateral tolerance range is set at (-0.01, 0.01) m.2. Structural Design of IRTMR

The structure of the IRTMR is designed to complete various sizes of road marking work, shown as Fig. 1. The overall length, width, and height of the IRTMR are 4 m, 2 m, and 1.5 m, respectively. The IRTMR mainly consists of A and B piston pumps, glass bead box, A and B paint barrels, radar, control box, pressured pump, power supply box, A and B spray nozzles, glass bead spray head, and other components.

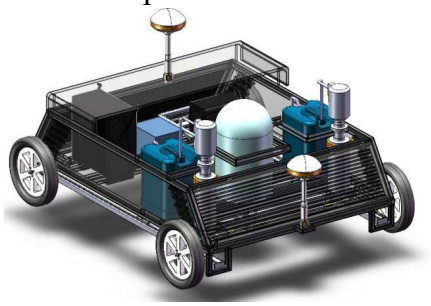

(a) Perspective view of intelligent road traffic marking robot

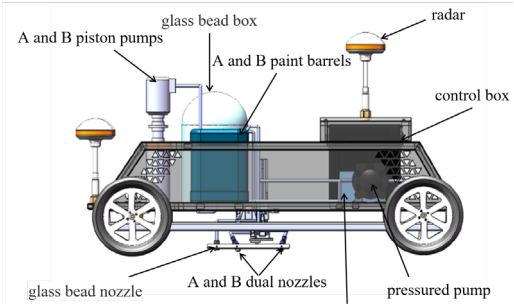

(b) IRTMR Structure Diagram

Fig. 1. Structure of the IRTMR

The map path information is imported into the radar sensor to achieve path recognition and obstacle sensing. Receiving and processing data from each sensor is realized through the preset procedures and logic of the control box. Two paint drums are connected to two plunger pumps to achieve the suction and discharge of A and B paints, the paint flows in the tube to the piston pumps, and the pressured pump enables the paint to be smoothly sprayed out of the nozzle to evenly coat the road surface by increasing the pressure in the paint system. In order to

improving driving safety, the glass beads sprayed by the glass bead nozzle are mixed into the sprayed paint to improve night visibility and enhance reflective performance of the road traffic signs and markings, The coordination action among IRTMR walking, plunger pump, A and B spray nozzles, and glass bead nozzle will be controlled to realize the adjustment of angle and height for A and B spray nozzles to achieve the road traffic marking application of different widths. The power supply provides electrical energy for the IRTMR.

As shown in Fig. 2, the A and B spray nozzles are used to spray two components (two-component materials) of coating simultaneously so that they do not mix before coming into contact. It is possible to keep the two coatings separate before mixing by using the A and B spray nozzles, thus effectively reducing the risk of clogging prior to reaction and ensuring uniformity of spraying. So the designed IRTMR has the advantages of uniform mixing, good spraying effect, high construction efficiency, reduced risk of clogging, high applicability and easier adjustment of the ratio compared to the single spray design [24]. In addition, the A, B spray nozzles and the glass bead spray nozzle are mounted on the frame through the three-coordinate module. The application of all kinds of characters and guiding arrows in the traffic marking can be realized by the control of the three-coordinate module.

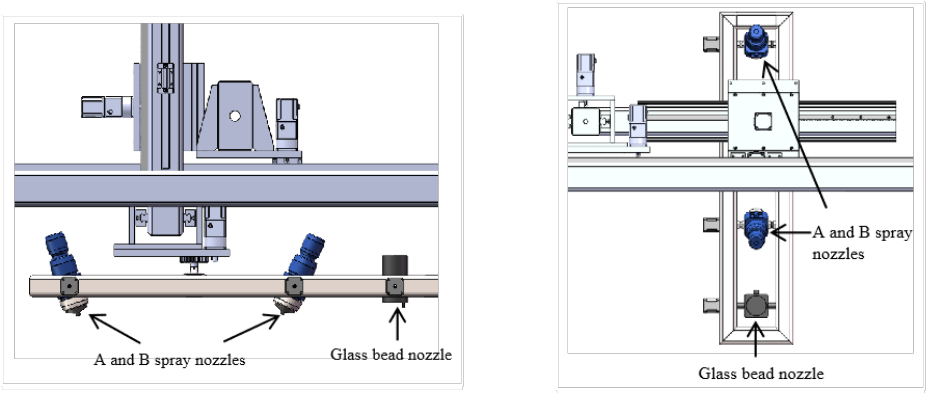

(a)Side view of double nozzle structure (b)Top view of double nozzle structure

Fig. 2. Spray nozzles structure

2 Kinematics and dynamics

2.1 *The kinematic model of IRTMR*

The inertial coordinate system *XOY* and the IRTMR coordinate system *xoy* are established as shown in Fig. 3. The yaw angle φ of the IRTMR is the angle

between the *x*-axis of the coordinate system and the *X*-axis of the coordinate system [25]. Where (X_r, Y_r) and (X_f, Y_f) are the coordinates of the midpoint of the rear axis and the midpoint of the front axis of the IRTMR in the inertial coordinate system, respectively. v_r is the speed of the IRTMR at the midpoint of the rear axis. l is the axis distance. R is the instantaneous steering radius at the midpoint of the rear axle. δ_f is the front wheel deflection angle.

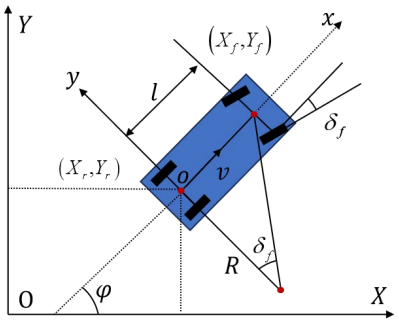

Fig. 3. Robot kinematic model diagram

The speed at the center (X_r, Y_r) of the rear axle can be written as:

$$v_r = \dot{X}_r \cos\varphi + \dot{Y}_r \sin\varphi \tag{1}$$

The kinematic constraint between the front axle and the rear axle can be written as:

$$\begin{cases} \dot{X}_f \sin(\varphi + \delta_f) - \dot{Y}_f \cos(\varphi + \delta_f) = 0 \\ \dot{X}_r \sin\varphi - \dot{Y}_r \cos\varphi = 0 \end{cases} \tag{2}$$

Combining Eq. (1) and Eq. (2), we can obtain:

$$\begin{cases} \dot{X}_r = v_r \cos\varphi \\ \dot{Y}_r = v_r \sin\varphi \end{cases} \tag{3}$$

According to the geometry of the front and rear wheels, it can be obtained:

$$\begin{cases} X_f = X_r + l\cos\varphi \\ Y_f = Y_r + l\sin\varphi \end{cases} \tag{4}$$

Substituting Eq. (3) and Eq. (4) into Eq. (2), the angular velocity of the pendulum can be solved as:

$$\omega = \frac{v_r}{l}\tan\delta_f \tag{5}$$

where, ω is the angular velocity of the IRTMR's traverse. At the same time, the steering radius R and the front wheel deflection angle δ_f can be obtained according to ω and the IRTMR speed v_r as, it can be written as:

$$\begin{cases} R = v_r / \omega \\ \delta_f = \arctan(l / R) \end{cases} \tag{6}$$

The kinematic model of the IRTMR is obtained according to Eq. (3) and Eq. (5), it can be written as:

$$\begin{bmatrix} \dot{X}_r \\ \dot{Y}_r \\ \dot{\varphi} \end{bmatrix} = \begin{bmatrix} \cos\varphi \\ \sin\varphi \\ \tan\delta_f / l \end{bmatrix} v_r \tag{7}$$

The kinematic model of the IRTMR can be further represented as:

$$\dot{\xi}_{\text{kin}} = f_{\text{kin}}\left(\xi_{\text{kin}}, \mathbf{u}_{\text{kin}}\right) \tag{8}$$

Where, $\xi_{\text{kin}} = [X_r, Y_r, \varphi]^{\text{T}}$ is the state quantity, $u_{\text{kin}} = \left[v_r, \delta_f\right]^{\text{T}}$ and $\left[v_r, \omega\right]$ are control quantity. Combining Eq. (5) with Eq. (7), the kinematic model of the IRTMR can be transformed into the following form:

$$\begin{bmatrix} \dot{X}_r \\ \dot{Y}_r \\ \dot{\varphi} \end{bmatrix} = \begin{bmatrix} \cos\varphi \\ \sin\varphi \\ 0 \end{bmatrix} v_r + \begin{bmatrix} 0 \\ 0 \\ 1 \end{bmatrix} \omega \tag{9}$$

2.2 *The Dynamics Model of IRTMR*

The following assumptions are proposed in the modeling dynamics of the IRTMR:

(1) Assume that the IRTMR moves on a flat surface, regardless of its motion in the vertical direction;

(2) Assume that both the suspension system and the IRTMR are rigid structures, the suspension motion and its effect on the coupling relationship are ignored;

(3) Only wheel characteristics in the purely sideways bias condition are considered, ignoring the interaction between transverse and longitudinal wheel forces;

(4) The effect of wheelbase on the turning radius can be neglected, so a monorail model is used to describe the motion of the IRTMR.

Based on the above assumptions, a model of transverse pendulum dynamics of the IRTMR can be obtained, as shown in Fig. 4. This model focuses on the motion of the IRTMR along the *x*-axis and *y*-axis, as well as the rotation around the *z*-axis

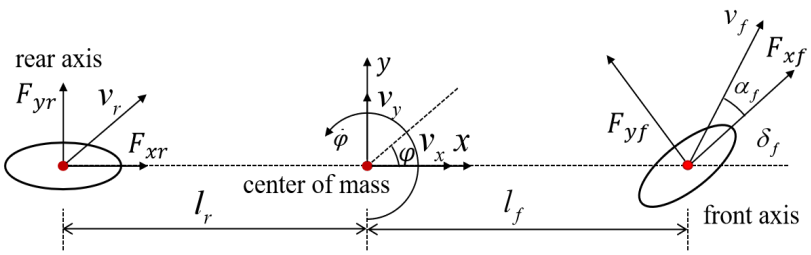

Fig. 4. Dynamics Model Diagram of IRTMR

Where, v_x and v_y are the longitudinal and lateral velocities of the center of mass in the IRTMR body coordinate system in Eq. 4, respectively, I_z is the moment of inertia of the IRTMR around the *z*-axis, l_f and l_r are the distances from the IRTMR 's center of mass to the front and rear axis, respectively, F_{yf} and F_{yr} are the combined wheel lateral forces acting on the front and rear axis of the IRTMR, respectively. F_{xf} and F_{xr} are the combined wheel longitudinal forces acting on the front and rear axis of the IRTMR, respectively, F_{dissp} is the combined force of resistance on the IRTMR in the longitudinal direction.

According to the nonlinear model of robot dynamics, the dynamics of the IRTMR can be expressed as:

$$m\left(\dot{v}_x - v_y\dot{\varphi}\right) = F_{xf}\cos\left(\delta_f\right) - F_{yf}\sin\left(\delta_f\right) + F_{xr} - F_{\text{dissp}} \tag{10}$$

$$m\left(\dot{v}_y + v_x\dot{\varphi}\right) = F_{xf}\sin\left(\delta_f\right) + F_{yf}\cos\left(\delta_f\right) + F_{yr} \tag{11}$$

$$I_z\ddot{\varphi} = l_f\left[F_{xf}\sin\left(\delta_f\right) + F_{yf}\cos\left(\delta_f\right)\right] - l_r F_{yr} \tag{12}$$

The lateral force is considered as an elastic force because its mathematical model resembles the form of elastic forces described by Hooke's Law. In vehicle dynamics, lateral forces are modeled in a specific manner. The force on the wheel can be expressed as:

$$F_{yf} = C_{yf}\alpha_f = C_{yf}\left(\delta_f - \left(V_y + a\dot{\varphi}\right)/V_x\right) \tag{13}$$

$$F_{yr} = C_{yr}a_r = C_{yr}\left(b\dot{\varphi} - V_y\right)/V_x \tag{14}$$

The degree of longitudinal sliding of the wheels is described by the slip ratios S_f and S_r, and the longitudinal forces between the tires and the road surface are directly affected by their values. In vehicle dynamics models, tire behavior under small slip ratios is approximated using the linear relationship. However, in practical control, nonlinear effects must be considered to optimize vehicle acceleration, braking, and stability.

On wet or slippery surfaces, when the critical slip ratio for lateral slip in small passenger cars exceeds 10%, the tire lateral force becomes insufficient to counteract the IRTMI's lateral motion demands, resulting in a significantly increased risk of loss of control.

$$F_{xf} = C_{xf}S_f \tag{15}$$

$$F_{xr} = C_{xr}S_r \tag{16}$$

Where, C_{yf} and C_{yr} are the deflection stiffness of the front and rear wheels, respectively. α_f and α_r are the lateral deflections of the front and rear wheels, respectively. C_{xf} and C_{xr} are the longitudinal stiffness of the front and rear wheels, respectively. S_f and S_r are the slip rates of the front and rear wheels, respectively. a and b are the distances from the center of mass to the front and rear axis, respectively.

$$m\dot{v}_y = -mv_x\dot{\varphi} + 2\left[\bar{C}_{\alpha f}\left(\delta_f - \frac{v_y + l_f\dot{\varphi}}{v_x}\right) + \bar{C}_{\alpha r}\frac{l_r\dot{\varphi} - v_y}{v_x}\right] \tag{17}$$

$$m\dot{v}_x = mv_y\dot{\varphi} + 2\left[C_{lf}s_f + \bar{C}_{\alpha af}\left(\delta_f - \frac{v_y + l_f\dot{\varphi}}{v_x}\right)\delta_f + C_{lr}s_r\right] \tag{18}$$

$$I_z\ddot{\varphi} = 2\left[l_f\bar{C}_{\alpha f}\left(\delta_f - \frac{v_y + l_f\dot{\varphi}}{v_x}\right) - l_f\bar{C}_{\alpha r}\frac{l_r\dot{\varphi} - v_y}{v_x}\right] \tag{19}$$

$$\dot{Y} = v_x\sin\varphi + v_y\cos\varphi \tag{20}$$

$$\dot{X} = v_x\cos\varphi - v_y\sin\varphi \tag{21}$$

The state quantities are selected as: $\xi = \left[V_x, V_y, \varphi, \dot{\varphi}, X, Y\right]$.The control volume is selected as: $u = \delta_f$ .The equation of state can be written as:

$$\dot{\xi} = f(\xi, u) \tag{22}$$

3 Path tracking control

3.1 *Kinematic control*

The kinematic equation of the IRTMR can be further expressed as:

$$\begin{cases} \dot{x} = v_x = v\cos\varphi \\ \dot{y} = v_y = v\sin\varphi \\ \dot{\varphi} = \dfrac{v\tan\delta}{l} \end{cases} \Rightarrow \begin{bmatrix} \dot{x} \\ \dot{y} \\ \dot{\varphi} \end{bmatrix} = \begin{bmatrix} v\cos\varphi \\ v\sin\varphi \\ \dfrac{v\tan\delta}{l} \end{bmatrix} = \begin{bmatrix} f_1 \\ f_2 \\ f_3 \end{bmatrix} \tag{23}$$

$\chi = [x, y, \varphi]^{\mathrm{T}}$ is selected as the state quantities. $u = [v, \delta]^{\mathrm{T}}$ is selected as the control volume. r is any reference point along the reference trajectory, the above equation can be rewritten as:

$$\dot{\chi}_r = f\left(\chi_r, u_r\right) \tag{24}$$

where $\chi_r = [x_r, y_r, \varphi_r]^{\mathrm{T}}$, $u_r = [v_r, \delta_r]^{\mathrm{T}}$. φ is the heading angle of the IRTMR, v is the speed of the IRTMR, δ is the steering angle of the IRTMR. The Taylor series expansion is applied to the above equation at the reference point, the following equation can be obtained:

$$\dot{\chi} = f\left(\chi_r, u_r\right) + \frac{\partial f(\chi,u)}{\partial \chi}(\chi - \chi_r) + \frac{\partial f(\chi,u)}{\partial u}(u - u_r) \tag{25}$$

The $\dot{\tilde{x}}$ in the state quantity error can be expressed as:

$$\dot{\tilde{\chi}} = \begin{bmatrix} \dot{x} - \dot{x}_r \\ \dot{y} - \dot{y}_r \\ \dot{\varphi} - \dot{\varphi}_r \end{bmatrix} = \begin{bmatrix} 0 & 0 & -v_r \sin\varphi_r \\ 0 & 0 & v_r \cos\varphi_r \\ 0 & 0 & 0 \end{bmatrix} \begin{bmatrix} x - x_r \\ y - y_r \\ \varphi - \varphi_r \end{bmatrix} + \begin{bmatrix} \cos\varphi_r & 0 \\ \sin\varphi_r & 0 \\ \dfrac{\tan\varphi_r}{l} & \dfrac{v_r}{l\cos^2\delta_r} \end{bmatrix} \begin{bmatrix} v - v_r \\ \delta - \delta_r \end{bmatrix} \tag{26}$$

where $A = \begin{bmatrix} 0 & 0 & -v_r \sin\varphi_r \\ 0 & 0 & v_r \cos\varphi_r \\ 0 & 0 & 0 \end{bmatrix}$, $B = \begin{bmatrix} \cos\varphi_r & 0 \\ \sin\varphi_r & 0 \\ \dfrac{\tan\varphi_r}{l} & \dfrac{v_r}{l\cos^2\delta_r} \end{bmatrix}$

Eq. (26) shows that state errors can form a linear state space. The forward Euler discretization equation of Eq. (26) can be expressed as:

$$\dot{\tilde{\chi}} = \frac{\tilde{\chi}(k+1) - \tilde{\chi}(k)}{T} = A\tilde{\chi} + B\tilde{u} \tag{27}$$

Eq. (27) can be further organized as follows:

$$\begin{aligned} \tilde{\chi}(k+1) &= (TA + E)\tilde{\chi}(k) + TB\tilde{u}(k) \\ &= \begin{bmatrix} 1 & 0 & -Tv_r \sin\varphi_r \\ 0 & 1 & Tv_r \cos\varphi_r \\ 0 & 0 & 1 \end{bmatrix} \tilde{\chi}(k) + \begin{bmatrix} T\cos\varphi_r & 0 \\ T\sin\varphi_r & 0 \\ T\dfrac{\tan\varphi_r}{l} & T\dfrac{v_r}{l\cos^2\delta_r} \end{bmatrix} \tilde{u}(k) \\ &= \tilde{A}\tilde{\chi}(k) + \tilde{B}\tilde{u}(k) \end{aligned} \tag{28}$$

3.2 *Dynamic control*

The dynamics model of the IRTMR will be investigated based on the steer small angles and wheel dynamics. By applying Newton's second law in the *y*-axis direction of the IRTMR, it can be concluded as:

$$ma_y = F_{yf} + F_{yr} \tag{29}$$

Where a_y is the lateral acceleration of the IRTMR. a_y consists of two components: $\ddot{y}$ is the acceleration generated by the lateral motion of the IRTMR along the *y*-axis, $v_x\dot{\varphi}$ is the centripetal acceleration resulting from the motion of the

pendulum. a_y can be expressed:

$$a_y = \ddot{y} + v_x\dot{\varphi} \tag{30}$$

$$m\left(\ddot{y} + v_x\dot{\varphi}\right) = F_{yf} + F_{yr} \tag{31}$$

The torque balance equation of the IRTMR around the *z*-axis can be written as:

$$I_z\ddot{\varphi} = F_{yf}l_f - F_{yr}l_r \tag{32}$$

Considering the small side deflection assumption, the two lateral forces acted on the wheel can be assumed as a linear relationship between the lateral force acted by the ground on the wheel (side deflection force) and the angle of side deflection of the wheel. The angle of side deflection of the front wheel is:

$$\alpha_f = \delta - \theta_{vf} \tag{33}$$

Where θ_{vf} is the angle between the direction of speed of the front wheel and the longitudinal axis of the IRTMR, δ is the front wheel steering angle.

The side deflection angle of the rear wheels is:

$$\alpha_r = -\theta_{vr} \tag{34}$$

Therefore, the lateral wheel forces on the front and rear wheels can be written as:

$$\begin{cases} F_{yf} = 2C_{\alpha f}\left(\delta - \theta_{vf}\right) \\ F_{yr} = -2C_{\alpha r}\theta_{vr} \end{cases} \tag{35}$$

The IRTMR can be treated as a rigid body, according to the rigid body kinematics, there is:

$$\begin{cases} \tan\theta_{vf} = \dfrac{v_y + \dot{\varphi}l_f}{v_x} \\ \tan\theta_{vr} = \dfrac{v_y - \dot{\varphi}l_r}{v_x} \end{cases} \Rightarrow \begin{cases} \theta_{vf} = \dfrac{v_y + \dot{\varphi}l_f}{v_x} \\ \theta_{vr} = \dfrac{v_y - \dot{\varphi}l_r}{v_x} \end{cases} \tag{36}$$

The transverse position, the rate of change of the transverse position, the transverse pendulum angle and the rate of change of the transverse pendulum

angle are considered as state variables, and the rate of change of the transverse position can be expressed as:

$$\frac{\mathrm{d}\dot{y}}{\mathrm{d}t} = \ddot{y} = \frac{F_{yf} + F_{yr}}{m} - v_x\dot{\varphi} \tag{37}$$

The rate of change of the transverse pendulum angle can be written as:

$$\frac{\mathrm{d}\dot{\varphi}}{\mathrm{d}t} = \ddot{\varphi} = \frac{F_{yf}l_f - F_{yr}l_r}{I_z} \tag{38}$$

The lateral dynamics model state space equations of the IRTMR can be expressed as:

$$\frac{\mathrm{d}}{\mathrm{d}t}\begin{bmatrix} y \\ \dot{y} \\ \varphi \\ \dot{\varphi} \end{bmatrix} = \begin{bmatrix} 0 & 1 & 0 & 0 \\ 0 & -\dfrac{2C_{\alpha f} + 2C_{\alpha r}}{mv_x} & 0 & -v_x - \dfrac{2l_fC_{\alpha f} - 2l_rC_{\alpha r}}{mv_x} \\ 0 & 0 & 0 & 1 \\ 0 & \dfrac{2C_{\alpha r}l_r - 2C_{\alpha f}l_f}{I_zv_x} & 0 & -\dfrac{2l_f^2C_{\alpha f} + 2l_r^2C_{\alpha r}}{I_zv_x} \end{bmatrix}\begin{bmatrix} y \\ \dot{y} \\ \varphi \\ \dot{\varphi} \end{bmatrix} + \begin{bmatrix} 0 \\ \dfrac{2C_{\alpha f}}{m} \\ 0 \\ \dfrac{2l_fC_{\alpha f}}{I_z} \end{bmatrix}\delta \tag{39}$$

3.3 *Path tracking control*

The MPC control algorithm is selected for the study. The path tracking control schematic is shown in Fig. 5, which demonstrates the modelling and control process of a system based on MPC. Firstly, the system model definition phase sets the curvature ρ and the relevant import parameters, including velocity, position, time interval, etc. Then the initial position and state are defined. Next, the user inputs the velocity v, steering angle δ, and imports the reference trajectory data. Subsequently, the *X* and *Y* coordinates of the reference trajectory are extracted, and the difference between these coordinates is calculated. Then, the reference heading angle can be calculated. After generating the actual heading angle, the state quantities will be updated, including the position (*x*, *y*), the heading angle ϕ and the time interval $\mathrm{d}t$. Next, the MPC controller is invoked, and the global variables are set. The loop index and the previous position will be initialized. By solving quadratic programming, the control strategy is optimized, and the final control result will be output.

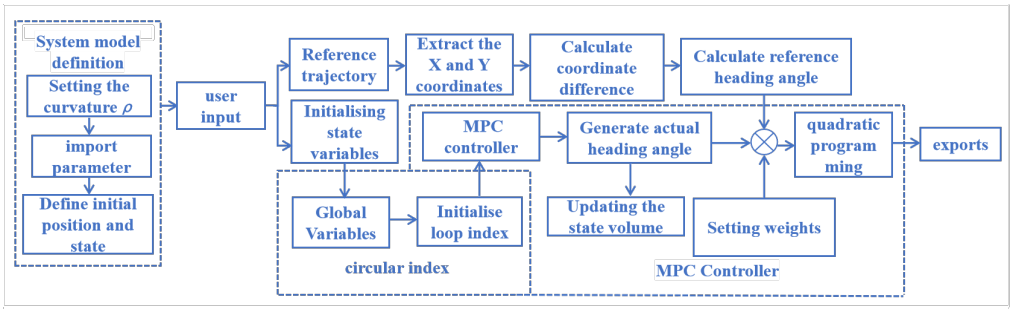

Fig. 5. Schematic diagram of path tracking control

The path tracking control flowchart of the MPC controller is shown in Fig. 6.

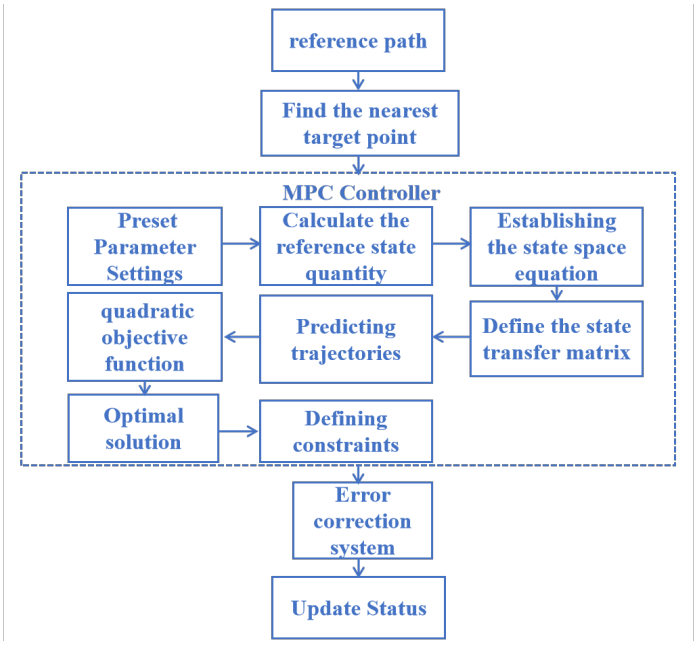

Fig. 6. MPC path tracking control flowchart

The control process is as follows: setting up a reference path and searching for a target point that determines whether the system has reached at the current moment. The control parameters and constraints can be pre-set to ensure that the system can achieve the expected performance and stability during the control process. Based on the reference trajectory and the current state of the system, the amount of the reference state of the system are calculated in order to guide the subsequent control operation. The state-space model is constructed to describe the dynamical behavior of the system, including state variables and input-output relationships. The control objective function is formulated, containing tracking

error and control increment to achieve optimal tracking of the reference trajectory. The state trajectory of the system at future moments and the corresponding increment of the control input can be predict using the state-space model.–The optimal sequence of control inputs can be obtained by solving the quadratic programming problem. In order to ensure that the actual state is as close as possible to the reference state, the error of the system need to be corrected in real-time. Finally, the actual state of the system will be updated according to the optimal control inputs.

4 Simulation analysis

The basic parameters of the designed IRTMR are shown in Table 1. In order to test the accuracy of the MPC path tracking control algorithm, the simulation and comparison experiments with, the pure Pursuit algorithm, Stanley algorithm, and LQR algorithm will be carried out in this study, respectively.

Table 1

Basic Parameters of the IRTMR

parameters	m (kg)	r(mm)	l (m)	l_f(mm)	l_r(mm)	$c_f\left(\mathrm{N\cdot rad^{-1}}\right)$	$c_r\left(\mathrm{N\cdot rad^{-1}}\right)$	$I_z\left(\mathrm{kg\cdot m^2}\right)$
value	500	285	3.2	1450	1750	66900	62700	4175

The simulation experiments are carried out with the trajectory tracking algorithms (pure pursuit and Stanley) based on the geometric model. The simulation results are shown in Fig. 7.

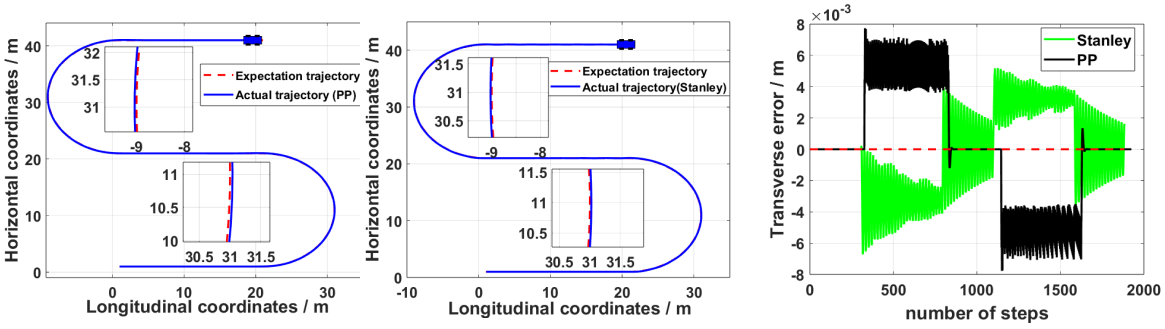

(a)Comparison chart of tracking effect (Pure Pursuit)

(b)Comparison chart of tracking effects (Stanley)

(c)Comparison of Lateral Error between Pure Pursuit and Stanley

Fig. 7. Simulation of Pure Pursuit and Stanley Algorithm

The results show that the root mean square errors (RMSE) of the Pure Pursuit algorithm and the Stanley algorithm are 0.003826 m and 0.002702 m, respectively, and the peak lateral errors (PLE) of the Pure Pursuit algorithm and the Stanley algorithm are 0.007774 m and 0.006718 m, respectively. The RMSE of the Stanley algorithm are 29.4% smaller than that of the Pure Pursuit algorithm.

Compared with the Stanley algorithm, the PLE of the Stanley algorithm is reduced by 13.5%. Therefore, the control accuracy of the Stanley algorithm is higher than the Pure Pursuit algorithm.

The simulation experiments on the trajectory tracking algorithms (LQR and MPC) based on kinematics and dynamics models are carried out, and the simulation results are shown in Fig. 8.

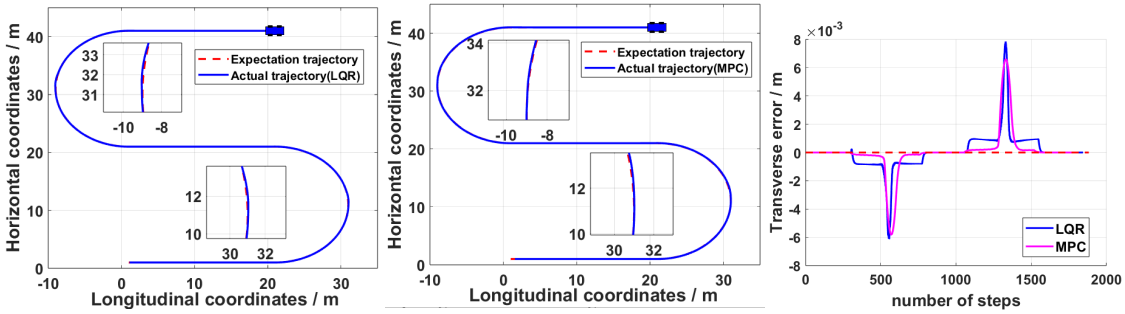

(a)Comparison chart of tracking effect (LQR)

(b)Comparison chart of tracking effect (MPC)

(c)Comparison of Lateral Error between LQR and MPC Algorithms

Fig. 8. Simulation of LQR and MPC Algorithm

The results show that the RMSE of LQR algorithm and MPC algorithm is 0.001336 m and 0.001319 m. the PLE of LQR algorithm and MPC algorithm are 0.007850 m and 0.006589 m, respectively. Compared with LQR algorithm, the RMSE and the PLE of MPC algorithm is reduced by 1.27% and 16.0%, respectively.

The simulation results of the pure Pursuit algorithm and the Stanley algorithm show that the Stanley algorithm has a lower control error; Compared with LQR algorithm, the MPC algorithm has a lower error and a better control effect.

In summary, it can be seen that the MPC algorithm has a smaller RMSE and PLE. The MPC algorithm can better control the lateral motion accuracy of the IRTMR. That is to say, the MPC algorithm has a better control effect, which can meet the requirements of the lateral motion trajectory tracking control accuracy of the IRTMR.

5 Conclusion

An IRTMR with two-component spraying is designed in this study. The kinematics and dynamics model of the IRTMR is established, and the path tracking control principle and the path tracking control process of MPC algorithm

are analyzed. After that the pure Pursuit algorithm based on geometric model, the Stanley algorithm and the LQR algorithm based on the kinematics and dynamics model and the MPC algorithm are simulated and experimented. The RMSE and PLE of the four algorithms are calculated respectively. The results show that the RMSE of the MPC algorithm is 0.001319 m, and the PLE is: 0.006589 m. Therefore, compared with the other three algorithms, the control effect of the MPC algorithm is the best.

The experimental results show that the MPC algorithm has a better path tracking control effect. It lays the foundation for the path tracking control research of the IRTMR prototype in the future.

Acknowledgement

This work was financially supported by Gansu Province Science and Technology Program Project Funding (No. 25CXGA076), Lanzhou Science and Technology Major Project under Grant (No. 2024-2-17), and Independent Project of Gansu Road & Bridge Construction Group (No.2023-02).

REFERENCES

[1] *Zhang Xin-yuan, Cheng Long.* Research on the Setting of Road Traffic Signs and Markings Based on the Characteristics of Urban Development the New Era [J]. Transportation Technology and Management, **vol**.4, **no.**18, 2023, pp.60-62.

[2] *E Xiao-yu, Meng Li-jun.* Development of Pneumatic High-Pressure Airless Cold Spray Road Marking Vehicle [J]. Road Machinery and Construction Mechanization, **vol**.1, **no**.38, 2004, pp.38-39.

[3] *Yuan Wei-qi, Wang Hui-li.* Research on the Detection Method and Device of the Reference Line for Road Marking Vehicles [J]. Instrument Technology and Sensors, **vol**.1, **no**.8, 2008, pp.101-103.

[4] *Liu Ya-jun, ZI Bin*, *Wang Zheng-yu, et al.* Research status and progress of key technologies for intelligent spraying robots [J]. Journal of Mechanical Engineering, **vol**.58，**no**.7, 2022, pp. 53-74.

[5] *XIA Jin-jun, Zhou Tao.* Design of a self-propelled road marking vehicle based on 3D road models [J]. Mechanical Design, **vol**.33, **no**.4, 2016, pp.113-115.

[6] *WEI Ming*. Introduction to Fully Automatic Highway Marking Robot [J]. Robot, **vol**.1, **no**.4, 1998, pp.57-63.

[7] *Jin M, Li J, Chen T, et al.* Method for the Trajectory Tracking Control of Unmanned Ground Vehicles Based on Chaotic Particle Swarm Optimization and Model Predictive Control[J]. Symmetry, **vol**.16, **no**.6, 2024, pp.708-708.

[8] *Yu Xiang-jun, Huai Yuan-hui, Yao Zong-wei, et al.* Key Technologies for Autonomous Driving of Engineering Vehicles [J]. Journal of Jilin University (Engineering Edition), **vol**.51, **no**.4, 2021, pp.1153-1168.

[9] *Zhou Jie-hua, Dai Ji-yang, Zhou Ji-qiang, et al.* Research on Path Planning and Trajectory Tracking Control of Mowing Robots for Large Airport Lawn [J]. Journal of Engineering Design, **vol**.26, **no**.2, 2019, pp.146-152.

[10] *Lu S, Liwei Z.* Trajectory Following Control of Modern Configurable Multi-Articulated Urban Bus Based on Model Predictive Control [J]. Sustainability, **vol**.14, **no**.24, 2022, pp.16619- 16619.

[11] *Yanxin N, Minglu Z, Xiaojun Z, et al.* Trajectory Tracking Control of Intelligent Electric Vehicles Based on the Adaptive Spiral Sliding Mode[J]. Applied Sciences, **vol**.11, **no**.24, 2021, pp.11739-11739.

[12] *Akguel, Muhammed, H. Bozma, et al.* RBOT-Design and Usage Manual. 2022.

[13] *Chen Hong-ying.* Spray Technology of Graco Push Water-based Coating [J]. Shanghai Chemical Industry, 2020, 45(01): 75.**vol**.45, **no**.1, 2020-, pp.643-651.

[14] *Liu Shi-liang, LI Hui, Wang Chuan, et al.* Research and Application of Development of Two-Component Waterborne Ultra-Thin Wear-Resistant Reflective Road Marking[J]. Shandong Jiaotong Keji, **vol**.1, **no**.4, 2024, pp.158-161.

[15] *LI fang, WEI Yong, CHEN Yue-wei, et al.* Design of MMA Two-Component Road Marking Coating Formula Based on Mixture Experimental Design and Its Performance [J]. Journal of Materials Science and Engineering, **vol**.42, **no**.26, 2024, pp.213-221+231.

[16] *Gu Donghai.* Analysis of the Application and Characteristics of Two-Component Road Marking Coatings [J]. Building Materials and Decoration, **vol**.1, **no**.19, 2017, pp.268-269.

[17] *Guan Lai-sheng.* Comparison of MMA Two-Component Road Marking Coating and Hot Melt Road Marking Coating [J]. Heilongjiang Transportation Science and Technology, **vol**.36, **no**.10, 2013, pp.155-157.

[18] *Song Li-fang, Wei Yong, Chen Yue-wei, et al.* Formula design and performance of MMA two-component marking coating based on mixed experimental design [J]. Journal of Materials Science and Engineering, **vol**.42, **no**.2, 2024, pp.213-221+231.

[19] *LI Bo-xiong, Wang Li-yong, SUN Peng, et al.* Research on Lateral Tracking Control of Unmanned Vehicles [J]. Mechanical Science and Technology, **vol**.43, **no**.2, 2024, pp.197-202.

[20] *Wang Fa-an, Wang Bo-yang, Zhang Zhao-guo, et al.* Adaptive preview tracking fuzzy control algorithm for tracked vehicles [J]. Journal of Agricultural Engineering, **vol**.40，**no**.10, 2024, pp.32-43.

[21] *Fu Jing-zhi, Yin Ze-fan, Liu Yun-ping, et al.* Research on unmanned vehicle path tracking based on improved pure tracking algorithm [J]. Mechanical Design, **vol**.39, **no**.2, 2022, pp.41-45.

[22] *ZHou Wei-qi, Zhao Yi-han, Liu Qing-chao, et al.* Lateral control strategy for vehicle path tracking based on improved LQR [J]. Journal of Huazhong University of Science and Technology (Natural Science Edition), **vol**. 52, **no**.3, 2024, pp.135-141.

[23] *Cui Bing-bo, SUN Yu, JI Feng, et al.* Research on the Path Tracking Algorithm of Agricultural Machinery Whole Field Based on Fuzzy Stanley Model [J]. Journal of Agricultural Machinery, **vol**.53, **no**.12, 2022, pp.43-48+88.

[24] *Song Li-fang, Wei Yong, Chen Yue-wei, et al.* Formula design and performance of MMA two-component marking coating based on mixed experimental design [J]. Journal of Materials Science and Engineering, **vol**.42, **no**.2, 2024, pp.213-221+231.

[25] *Gong Jian-wei.* Model Predictive Control of Autonomous Vehicles, Second Edition [M].Beijing: Beijing Institute of Technology Press, 2020.